Predictive lumped model for a tunable bistable piezoelectric energy harvester architecture

Aya Benhemou, David Gibus, Thomas Huguet, Adrien Morel, Quentin Demouron, Camille Saint-Martin, Emile Roux, Ludovic Charleux, Adrien Badel

IOP Publishing Smart Materials and Structures
Smart Mater. Struct. **33** (2024) 045033 (15pp) https://doi.org/10.1088/1361-665X/ad2c6a

Predictive lumped model for a tunable bistable piezoelectric energy harvester architecture

Aya Benhemou[1,*], David Gibus[1], Thomas Huguet[2], Adrien Morel[1], Quentin Demouron[1], Camille Saint-Martin[1], Emile Roux[1], Ludovic Charleux[1] and Adrien Badel[1]

[1] SYMME, University Savoie Mont-Blanc, F-74000 Annecy, France
[2] LAPLACE, Université de Toulouse, CNRS, INPT, UPS, F-31071 Toulouse, France

E-mail: aya.benhemou@univ-smb.fr

Received 10 November 2023, revised 9 January 2024
Accepted for publication 22 February 2024
Published 28 March 2024

Abstract

In this article, we propose the modelling of a tunable bistable piezoelectric energy harvester (or BPEH) architecture. The latter is a type of ambient energy converter that continues to gain attention due to their wideband frequency response. As the non-linear dynamics of BPEHs imply significant modeling complexity, dynamic lumped models are necessary to predict BPEHs' dynamic response and should fit the type of architecture studied. The BPEH architecture of interest uses post-buckled beams to create bistability and an amplified piezoelectric actuator (or APA) to convert the ambient vibrations. To date, no dynamic lumped models have been found in existing literature that account for both the electromechanical conversion and the dynamic behavior of buckled beams, with a specific focus on their axial and bending stiffness, for this BPEH architecture. Additionally, the proposed BPEH architecture offers buckling level tunability, which is achieved using an additional APA. Hence, the aim of this paper is to propose a new lumped model for a BPEH architecture that considers the effect of the post-buckled beams' stiffness and of the additional APA through an elasticity factor $\overline{\kappa}$. This lumped model is established using Euler Lagrange equations and is experimentally validated on a tunable BPEH prototype. This validation shows an average relative error below 6% between the model predictions and experimental dynamic response of the prototype to an ascending frequency sweep, compared to an average relative error that is around 14% for the model proposed in literature. Moreover, numerical simulations using the proposed model lead to the conclusion that there is an optimal elasticity factor $\overline{\kappa}$ that ensures the maximum power output while maintaining the frequency bandwidth.

Keywords: piezoelectric energy harvester, bistability, dynamic lumped model, post-buckled beams

1. Introduction

The interest in wireless sensor networks (or WSNs) has significantly risen in the past decade. This is due to the fact that those networks can enable real time monitoring of the physical condition of a wide range of structures, such as aircrafts, medical apparatus or even industrial machinery [1, 2]. The energy consumption of sensor nodes is one of the challenges for this promising technology.

The conventional way to power these nodes is chemical batteries. Since these batteries have a limited amount of energy, and therefore a short life cycle, it is relevant to use the existing energy in the environment of the monitored structures as

* Author to whom any correspondence should be addressed.

an alternative [3, 4]. One commonly studied example is vibration energy harvesting, which consists of converting ambient mechanical energy into electric energy [5], using electromagnetic induction [6], electrostatic mechanisms [7, 8], or piezoelectric components coupled with mechanical resonators [9]. Piezoelectric energy harvesters (or PEHs) will be the focus of this work.

The use of linear mechanical resonators for PEHs was first investigated in the early 2000s by Roundy and Wright [10], due to the simplicity of modeling and design they offer. Nevertheless, it has been shown that linear resonators are not suitable for all ambient vibrations [11], and that a wider frequency bandwidth is preferred for ambient vibrations [12].

One of the most promising methods investigated for the purpose of enlarging the PEHs' bandwidth is the introduction of a non-linearity in the oscillating structure [13–15], such as bistability [16]. Bistability is a type of non-linearity that implies the existence of two stable equilibrium positions in a given system.

This type of non-linearity is achieved by two methods. The first method is referred to as magnetic interaction or magnetic coupling and consists of installing magnets on and around the mechanical resonator to create two equilibrium positions [17]. Magnet based bistability in BPEH can either be achieved using attractive mechanisms [18], but is most commonly achieved using repulsive mechanisms [19]. More recent architectures of this type use both to optimize the elastic potential [20], or use beams with complex shapes instead of simple cantilever beams to increase the strain and thus the electromechanical coupling of the BPEH [21].

Despite the advances in this type of BPEH, the use of magnets implies higher volumes in the BPEH, which leads us to focus on the second widely used method to achieve bistability. This method consists of introducing a pre-compression in thin beams or plates, which causes the structure to buckle. Apart from simple buckled structures [22, 23], there are architectures that use optimized beam shapes to enhance performance at low accelerations [24], and more complex bistable mechanisms that exploit different stress modes [25] also exist. The advantage of this type of BPEH structures is the smaller volume they ensure. We consequently focus on bistability based buckling and how to design these types of BPEH in the following study.

The aforementioned solution calls for more intricate modeling that can be either inaccurate, either inappropriate for some architectures. The purpose of this paper is to present a model dedicated to the design and the prediction of the dynamic behavior of a high performance bistable piezoelectric harvester that uses post-buckled beams to create bistability and a flextensional device to convert the vibration into electric energy.

Concerning the modelling of these types of BPEH, a number of models were proposed in literature. Vangbo first investigated the modeling of double-clamped post-buckled beams with a centered actuation, proposing a Lagrangian approach to study their static behavior [26] which considered the beams' bending and axial extension. This approach was then extended by others to propose design approaches as well as elastic static analytical models for post-buckled beams with an off-centered actuation [27, 28]. Static modeling results are, however, insufficient to determine how post-buckled beams affect the dynamic behavior of a bistable vibrating structure, such as bistable piezoelectric energy harvesters (or BPEHs).

Hence, dynamic lumped models have been developed for dynamic structures that use post-buckled beams. An interesting example is the model developed and experimentally verified by Saif for a tunable MEMS architecture in the year 2000 [29]. It does not, however, take into consideration the electromechanical aspect of the device which is a key element of the study of BPEHs. Dynamic electromechanical lumped models were thus developed for BPEH architectures.

The one proposed by Cottone *et al* in 2012 [30] comes to mind as it describes the effect of the beams in the electromechanical equations for an architecture that uses piezoelectric patches laminated on the bistable beams of the BPEH [31]. More recently, a more detailed model for BPEH using post-buckled beams with piezoelectric patches has been proposed by Karadarakos *et al* [32]. The latter proposes a more intricate model to account for a wider range of mechanical deformations and conversion modes in the piezoelectric element, which allows for more accurate predictions, but also requires more computational power and a longer computation time.

In addition, the effects of the post-buckled beams for this type of architecture differ from those of beams that incorporate the piezoelectric element in a different way, more particularly, when exploiting a different electromechanical coupling mode (or ECM) such as the 3-3 mode using flextensionnal devices [33].

Two piezoelectric ECMs are commonly used in electromechanical systems; the 3-1 mode, where the mechanical strain is perpendicular to the polarization vector, and the 3-3 mode, which uses stacks with interdigitated (IDT) electrodes and for which strain and polarization are collinear. The benefit of exploiting 3-3 ECMs in the piezoelectric element as opposed to the 3-1 ECMs, solicited in BPEH architectures that use piezoelectric patches such as Qian *et al*'s [25] or Chen *et al*'s [24] architectures, is to obtain a higher electromechanical coupling level as discussed by Kim *et al* [31], which is a definite advantage in the context of vibration energy harvesting.

A notable contribution to the modeling of this type of architecture, taking advantage of the 3-3 ECMS, is Liu *et al*'s model for a BPEH that uses amplified piezoelectric actuators (or APAs), also referred to as flextensional devices, for energy harvesting purposes [34]. The effect of the bending strain contribution of the post-buckled beams was included in Liu *et al*'s model [35], and was proven to have no effect on the electromechanical coupling of the BPEH for the architecture investigated. It is unclear, however, whether the axial stiffness, which represents the axial extension strain modes of the beams, influences the BPEH's dynamic behavior for structures that use 3-3 ECMs. We investigated the effect of this axial stiffness for a non-tunable BPEH architecture in a previous article [36]. It was demonstrated that for this type

of BPEH architecture, relatively low values of the axial stiffness of the beams can have a detrimental effect on the BPEH's power output.

Another contribution concerning this type of BPEH architecture is proposed by Huguet *et al* [37], in which a BPEH architecture using an additional APA to achieve orbit jumps, a method used to enhance the BPEH's performance, was suggested. Unfortunately, in this contribution, the lumped model proposed does not account for the effect of the buckled beams or that of the additional APA used to tune the buckling level.

So far, no work in literature has proposed a model for BPEHs using APAs and post-buckled beams that considers the influence of beam axial and flexural stiffness as well as the stiffness of any extra APA. The presented work aims to propose a lumped model for a tunable BPEH architecture, appropriate for testing orbit jump strategies, which accounts for the use of APAs for energy harvesting and tuning purposes, as well as the post-buckled beams' effect on the dynamic behavior of the harvester. Unlike previous contributions, this model allows us to predict how each of the previously cited components affects the dynamic response of the BPEH.

This article is organized in the following manner: the second section establishes the dynamic lumped model of the BPEH architecture studied. The third section presents the experimental validation of the proposed lumped model, using an existing BPEH prototype. The fourth section exploits the proposed lumped model to study how the beams and the tuning APA can affect the dynamic response of the BPEH using numerical simulations.

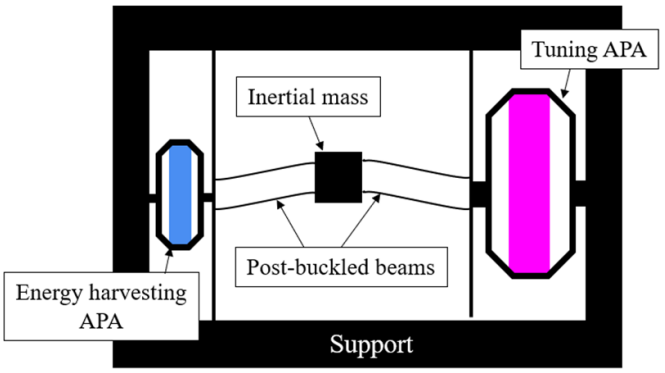

Figure 1. A schematic of the studied BPEH architecture that includes an inertial mass, 4 post-buckled beams, one APA for energy harvesting and an additional APA for tuning the buckling level.

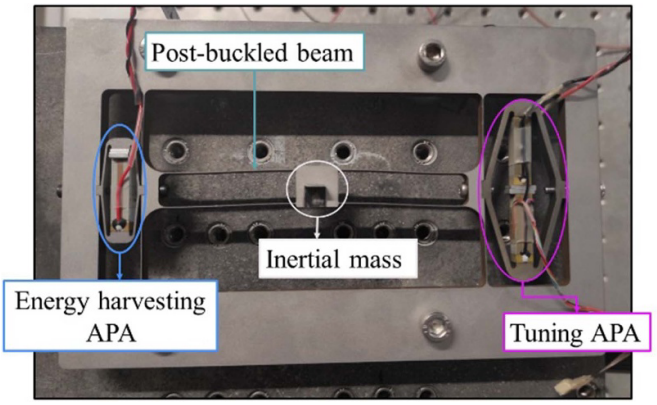

Figure 2. Image of the BPEH prototype used for the experimental validation, that includes a 6*g* inertial mass, 4 post-buckled beams and two APAs for energy harvesting (APA120S) and tuning (APA100M).

2. A dynamic lumped model for the tunable BPEH architecture

2.1. The BPEH architecture presentation

The BPEH architecture studied in this paper is similar to Huguet *et al*'s BPEH prototype described in [37], shown in the diagram in figure 1 and in the prototype image in figure 2. It includes an inertial mass, four bistable post-buckled beams used to create bistability and two APAs. Four buckled beams were chosen instead of two in order to prevent in plan rotations of the inertial mass.

One of the two APAs is used for energy harvesting. This APA generates power upon the inertial mass's movement and is linked to a simple resistance load for the rest of the study, for simplification purposes. The harvested energy will be evaluated as the energy dissipated in the resistor.

The second APA is used as an actuator to adjust the buckling level of the beams. When used as an actuator, the APA is in compression along the horizontal axis when the applied tuning voltage is positive, and in extension when this voltage is negative.

The aim of this architecture is to make it easy to tune the buckling level, so that the model can be validated at different buckling levels. For a given real-world application, this second APA could be removed.

2.2. The BPEH dynamic lumped model formulation

The modelling approach presented in this paper is illustrated in the schematic shown in figure 3.

As shown in figure 3, we attach a fixed Cartesian reference frame $(\overrightarrow{e_x}, \overrightarrow{e_y})$ to the BPEH. The variable x represents the displacement of the inertial mass M in the $\overrightarrow{e_x}$ direction, while D represents the damping coefficient, and L the mass frame distance. The variables K, C_p and α respectively represent the stiffness, capacitance and force factor of the energy harvesting APA.

The axial extension and bending stiffnesses of each beam are noted K_a and K_b. In addition, the effect of the tuning APA is added by considering its stiffness K_2, capacitance C_{p_2} and force factor α_2.

The voltage and electric current of the energy harvesting and tuning APAs are respectively represented by the variables (v, I) and (v_2, I_2). As depicted in figure 3, the energy harvesting APA is connected to a resistance load denoted by R, whereas the tuning APA is connected to a voltage source. Furthermore, the variable γ corresponds to the acceleration of the ambient vibration. The amplitude of this acceleration will be referred to as γ_M.

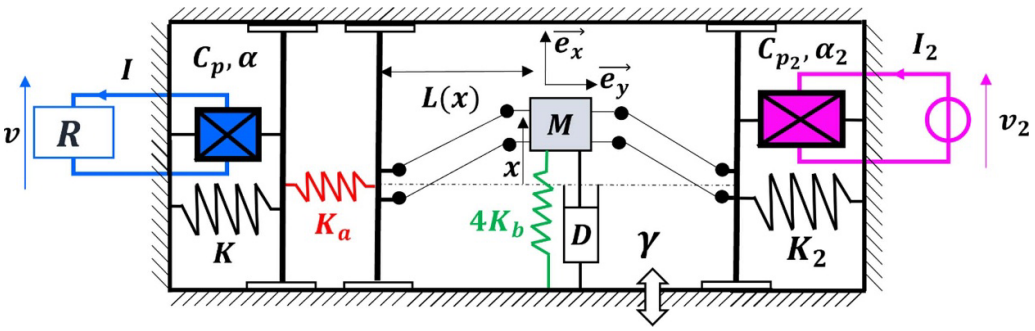

Figure 3. Schematic representation of the Lumped model proposed in this paper to describe the tunable BPEH architecture represented in figures 1 and 2.

Prior to entering detailed modelling considerations of the problem under study, some basic prerequisites and assumptions are introduced:

(1) The inertial mass M is considered moving along the $\vec{e_x}$ direction only, which is valid when considering the displacement of the mass to be very small compared to the length of the beams ($x << L$).
(2) It is assumed that the strain of the 4 identical post-buckled beams is the same. The strain contributions of the post-buckled beams are accounted for by adding springs for their bending and axial extension stiffnesses, respectively named K_b and K_a that will thus have an identical value from one beam to another.
(3) The bending stiffness K_b of the four identical beams act in parallel on the mass and oppose its displacement along the $\vec{e_x}$ direction. They can thus be modelled with an equivalent stiffness $4K_b$ as shown in figure 3. The axial extension stiffness K_a oppose the mass's movement along the $\vec{e_y}$ direction. Along this axis the axial extension stiffness of the beams adds up on both sides of the mass, but are in series when considering both symmetrical sides. The global equivalent axial extension stiffness K_a is then equal to the axial extension stiffness of one beam.
(4) The movements of the inertial mass in the $\vec{e_x}$ direction induces a displacement of the axial extension stiffness spring K_a and of both APAs in the $\vec{e_y}$ direction. For a displacement x of the inertial mass, a displacement variation ΔL in the $\vec{e_y}$ direction occurs. The expression of this displacement variation ΔL is described in (1). The Pythagorean theorem is used to derive this formula since the model's linkages enabling the mass's movement are assumed to be infinitely rigid. The strain on the beams is considered independently using the springs for the bending and axial extension stiffnesses K_b and K_a

$$\Delta L = 2(L - L(x)) = 2L - 2\sqrt{L^2 + x_0^2 - x^2}. \tag{1}$$

The latter is the difference between the mass-frame distance L when the inertial mass's displacement is equal to the buckling level ($x = x_0$), and the mass-frame distance $L(x)$ for a given inertial mass displacement ($x \neq x_0$).

The displacement variation of the energy harvesting APA is denoted by y_K, and the displacement variation of the tuning APA is denoted by y_{K_2}, while y_{K_a} represents the displacement variation of the axial extension spring. The sum of these displacement variations is evidently equal to the total displacement variation ΔL. This thought is expressed in (2)

$$\Delta L = y_{K_a} + y_k + y_{K_2}. \tag{2}$$

With these considerations made, we can now move on to the formulation of the lumped model's equations. As a classical method, the Euler–Lagrange approach to modelling is used to deduce the governing equations of the structure.

The generalized coordinates considered are the position of the mass x, the variables y_K and y_{K_2} that represent the displacement variation of the energy harvesting and tuning APAs upon the inertial mass's movements and two voltage related coordinates λ and λ_2 as $\dot{\lambda} = v$ and $\dot{\lambda}_2 = v_2$. The corresponding Euler–Lagrange balance is described by the equation system (3)

$$\begin{cases} M\gamma - D\dot{x} = \frac{\mathrm{d}}{\mathrm{d}t}\left(\frac{\partial \mathbb{L}}{\partial \dot{x}}\right) - \frac{\partial \mathbb{L}}{\partial x} \\ 0 = \frac{\mathrm{d}}{\mathrm{d}t}\left(\frac{\partial \mathbb{L}}{\partial \dot{y}_K}\right) - \frac{\partial \mathbb{L}}{\partial y_K} \\ 0 = \frac{\mathrm{d}}{\mathrm{d}t}\left(\frac{\partial \mathbb{L}}{\partial \dot{y}_{K_2}}\right) - \frac{\partial \mathbb{L}}{\partial y_{K_2}} \\ -I = \frac{d}{\mathrm{d}t}\left(\frac{\partial \mathbb{L}}{\partial \dot{\lambda}}\right) - \frac{\partial \mathbb{L}}{\partial \lambda} \\ -I_2 = \frac{\mathrm{d}}{\mathrm{d}t}\left(\frac{\partial \mathbb{L}}{\partial \dot{\lambda}_2}\right) - \frac{\partial \mathbb{L}}{\partial \lambda_2} \end{cases} \tag{3}$$

The Lagrangian function $\mathbb{L}$ of the system is given by equation (4)

$$\mathbb{L} = T - S_{4K_b} - S_K - S_{K_a} - S_{K_2} + W_c. \tag{4}$$

The term T represents the kinetic energy of the inertial mass. The variables S_{4K_b}, S_K, S_{K_a} and S_{K_2} represents the elastic energy stored in the springs considered, shown in the lumped model schematic in figure 3. The variable W_c is the piezoelectric co-energy that exists in both APAs. The equations (5)–(10) define the expressions of these terms

$$T = \frac{1}{2}M\dot{x}^2 \tag{5}$$

$$S_{K_a} = \frac{1}{2}K_a(\Delta L - y_K - y_{K_2})^2 \tag{6}$$

$$S_K = \frac{1}{2}Ky_K^2 \tag{7}$$

$$S_{K_2} = \frac{1}{2}K_2 y_{K_2}^2 \tag{8}$$

$$S_{4K_b} = \frac{1}{2}\left(4K_b x^2\right) \tag{9}$$

$$W_c = \frac{1}{2}C_p v^2 + \alpha v y_K + \frac{1}{2}C_{p_2}v_2^2 + \alpha_2 v_2 y_{K_2}. \tag{10}$$

When combining the last equations, the Euler–Lagrange balance for the present BPEH architecture takes the form:

$$\begin{cases} M\gamma - D\dot{x} = M\ddot{x} + 4K_b x + \frac{K_a(\Delta L - y_K)2x}{\sqrt{L^2+x_0^2-x^2}} \\ 0 = Ky_k - K_a(\Delta L - y_k - y_{K_2}) - \alpha v \\ 0 = K_2 y_{K_2} - K_a(\Delta L - y_k - y_{K_2}) - \alpha_2 v_2 \\ -I = C_p\dot{v} + \alpha\dot{y}_K \\ -I_2 = C_{p_2}\dot{v}_2 + \alpha_2\dot{y}_2[6pt] \end{cases}. \tag{11}$$

The second and third equations of the system described in (11) give way to the expressions of the displacement variations y_K and y_{K_2} as functions of the other generalized coordinates considered. These expressions are given by (12) and (13)

$$y_K = \frac{\alpha_2 v_2 - \frac{\alpha K_a}{K+K_a}v + \frac{KK_a}{K+K_a}\Delta L}{\frac{KK_a}{K_a+K} + K_2} \tag{12}$$

$$y_{K_2} = \frac{KK_a}{K+K_a}\left(1 - \frac{\left(\frac{K_aK}{K+K_a}\right)}{K_2 + \left(\frac{K_aK}{K+K_a}\right)}\right)\Delta L + \frac{1 + \frac{\left(\frac{K_a}{K+K_a}\right)}{K_2+\left(\frac{K_aK}{K+K_a}\right)}}{K+K_a}\alpha v - \frac{\left(\frac{K_a}{K+K_a}\right)}{K_2 + \left(\frac{K_aK}{K+K_a}\right)}\alpha_2 v_2. \tag{13}$$

In order to facilitate the development and interpretations of the final equation system, the expression of an equivalent stiffness K_{eq} is introduced, as shown in equation (14)

$$K_{\text{eq}} = \frac{\left(\frac{K_aK}{K+K_a}\right)K_2}{K_2 + \left(\frac{K_aK}{K+K_a}\right)}. \tag{14}$$

When injecting equations (12) and (13) in the Euler–Lagrange balance, we obtain the equation system described in (15)

$$\begin{cases} M\ddot{x} + 4K_b x + \frac{K_{\text{eq}}\left(2L - 2\sqrt{L^2+x_0^2-x^2}\right)2x}{\sqrt{L^2+x_0^2-x^2}} + \frac{K_{\text{eq}}}{K}\alpha v\frac{2x}{\sqrt{L^2+x_0^2-x^2}} - \frac{K_{\text{eq}}}{K_2}\alpha_2 v_2\frac{2x}{\sqrt{L^2+x_0^2-x^2}} = M\gamma - D\dot{x} \\ C_p\dot{v} - \alpha\left(\frac{K_{\text{eq}}}{K}\right)\frac{2x\dot{x}}{\sqrt{L^2+x_0^2-x^2}} + \frac{1+\frac{K_aK_{\text{eq}}}{KK_2}}{K+K_a}\alpha^2\dot{v} - \frac{K_{\text{eq}}}{K_2K}\alpha_2\alpha\dot{v}_2 = -I \\ C_{p_2}\dot{v}_2 + \alpha_2^2\frac{\dot{v}_2}{K_2+\frac{KK_a}{K+K_a}} - \frac{\alpha\alpha_2K_{\text{eq}}}{KK_2}\dot{v} + \frac{K_{eq}}{K_2}\frac{2x\dot{x}}{\sqrt{L^2+x_0^2-x^2}} = -I_2 \end{cases}. \tag{15}$$

Since the displacements of the mass and buckling level are small with respect to L, a Taylor expansion of the first order can be applied on the terms of the equation system described in (15), as shown by (19)

$$\begin{aligned}(x_0 \ll L,\ x \ll L) \Rightarrow \frac{x_0^2 - x^2}{L^2} \ll 1 \Rightarrow \sqrt{1 + \frac{x_0^2-x^2}{L^2}} \\ \approx 1 + \frac{x_0^2-x^2}{2L^2} + o\left(\frac{x_0^2-x^2}{L^2}\right).\end{aligned} \tag{16}$$

The application of the Taylor expansion developed in (16) gives way to an equation system that includes a mechanical Duffing-type equation as well as two electrical equations as seen in (17)

$$\begin{cases} M\gamma = M\ddot{x} - 2K_{\text{eq}}\left(\frac{2K_{\text{eq}}x_0^2}{L^2} - 4K_b - \frac{2\alpha_{eq_2}v_2}{L}\right)x + \frac{2K_{\text{eq}}x^3}{L^2} \\ \qquad + D\dot{x} + \frac{2\alpha\left(\frac{K_{\text{eq}}}{K}\right)xv}{L} \\ I = \frac{2\alpha\bar{\kappa}x\dot{x}}{L} - \left(C_p + \frac{1+\frac{K_aK_{\text{eq}}}{KK_2}}{K+K_a}\alpha^2\right)\dot{v} + C_{\text{eq}}\dot{v}_2 \\ I_2 = \frac{2\alpha_2(1-\bar{\kappa})x\dot{x}}{L} - \left(C_{p_2} + \frac{\alpha_2^2}{K_2+\frac{KK_a}{K+K_a}}\dot{v}_2\right) + \frac{\alpha\alpha_2K_{\text{eq}}}{K_2K}\dot{v} \end{cases}. \tag{17}$$

The writing of the equation system given by (19) is further simplified by introducing a few variables that depend on the structural parameters.

The first variable considered appears when rewriting the linear reaction force of the BPEH as shown in (18)

$$\left(\frac{2K_{\text{eq}}x_0^2}{L^2} - 4K_b - \frac{2\alpha_{\text{eq}_2}v_2}{L}\right)x = \frac{2K_{\text{eq}}}{L^2}x_{01}^2 x. \tag{18}$$

This variable noted x_{01} is representative of a new buckling level written in terms of the ideal buckling level x_0 and of the influence of the bending stiffness K_b and tuning APA's compression that varies with the voltage v_2. The expression of this buckling level x_{01}, which will be referred to as the actual buckling level as it is the one observed experimentally, is given by (19)

$$x_{01} = \sqrt{\left(x_0^2 - \frac{2K_bL^2}{K_{\text{eq}}} - \frac{\alpha_{\text{eq}_2}v_2L}{K_{\text{eq}}}\right)}. \tag{19}$$

The second variable introduced is a correction factor that will be referred to as the elasticity factor $\bar{\kappa}$ for the rest of the study. This variable account for the elastic energy stored in the tuning APA and axial extension stiffness spring K_a of the beams. The expression of the elasticity factor $\bar{\kappa}$ is given by (20)

$$\overline{\kappa} = \frac{1}{1 + \frac{K}{\frac{K_aK_2}{K_2+K_a}}}. \tag{20}$$

In addition, the equivalent capacitances of the energy harvesting APA and tuning APA, respectively symbolized $C_{p_{\text{eq}}}$ and $C_{p_{2_{\text{eq}}}}$, as well as the additional capacitance C_{eq} are given by (21)–(23)

$$C_{p_{\text{eq}}} = \frac{1 + \frac{K_aK_{\text{eq}}}{KK_2}}{K + K_a}\,\alpha^2 \tag{21}$$

$$C_{p_{2_{\text{eq}}}} = \frac{\alpha_2^2}{K_2 + \frac{KK_a}{K+K_a}} \tag{22}$$

$$C_{\text{eq}} = \frac{\alpha\alpha_2\bar{\kappa}}{K_2}. \tag{23}$$

The capacitances $C_{p_{\text{eq}}}$ and $C_{p_{2_{\text{eq}}}}$ account for the change in boundary conditions of the APAs when fixed to the rest of the BPEH, and are added to the capacitances C_p and C_{p_2} respectively measured for the energy harvesting APA and tuning APA for free–free boundary conditions. The capacitance C_{eq} accounts for the existence of both APAs in the structure.

The equation system given by (24) stems from applying the Taylor expansion (see equation (16)) and considering the previously described variables

$$\begin{cases} M\gamma = M\ddot{x} - 2K\bar{\kappa}\frac{x_{01}^2}{L^2}x + \frac{2K\bar{\kappa}x^3}{L^2} + D\dot{x} + \frac{2\alpha\bar{\kappa}xv}{L} \\ I = \frac{2\alpha\bar{\kappa}x\dot{x}}{L} - \left(C_p + C_{p_{\text{eq}}}\right)\dot{v} + C_{\text{eq}}\dot{v}_2 \\ I_2 = \frac{2\alpha_2(1-\bar{\kappa})x\dot{x}}{L} - \left(C_{p_2} + C_{p_{2_{\text{eq}}}}\right)\dot{v}_2 + C_{\text{eq}}\dot{v}[6pt] \end{cases}. \tag{24}$$

The purpose of this article is to investigate the response of the BPEH architecture for different buckling levels, and to compare the experimental response with the predictions of the model. For this purpose, the value of the actual buckling level x_{01} is modified by varying the tuning voltage v_2 before each test, which consists of observing the dynamic response of the BPEH.

Consequently, for the study carried out in this paper, the actual buckling level is kept constant when the BPEH is subjected to a given excitation of amplitude γ_M.

The voltage applied to the tuning APA is then kept constant ($\dot{v}_2 = 0,\ v_2 = V_2$). The expression for the actual buckling level is therefore that given by (25). The third equation in the system of equation (24) is thus useless for the following study, as it only provides information on the current that flows through the tuning APA as a function of the BPEH's motion

$$x_{01} = \sqrt{\left(x_0^2 - \frac{2K_bL^2}{K_{\text{eq}}} - \frac{\alpha_{eq_2}V_2L}{K_{\text{eq}}}\right)}. \tag{25}$$

The two remaining equations given by (26) describe a BPEH with a tunable buckling level that depends on the value set to the tuning APA voltage V_2.

Additionally, for the APAs considered in this paper, the additional capacitances $C_{p_{\text{eq}}}$, $C_{p_{2\text{eq}}}$ and C_{eq} that account for the difference in boundary conditions in the energy conversion process of the APAs are negligible in comparison to the capacitances C_p and C_{p_2} of the free–free APA configuration. The terms containing these variables are therefore considered negligible in both electric equations, and the simplified equation system given by (26) is finally found

$$\begin{cases} M\gamma = M\ddot{x} - 2K\bar{\kappa}\frac{x_{01}^2}{L^2}x + \frac{2K\bar{\kappa}}{L^2}x^3 + D\dot{x} + \frac{2\alpha\bar{\kappa}}{L}xv \\ I = \frac{2\alpha\bar{\kappa}}{L}x\dot{x} - C_p\dot{v} \end{cases} \tag{26}$$

The system of equation (26) describes the oscillations of an inertial mass attached to a nonlinear spring and a linear damper, with additional nonlinear electromechanical coupling terms. These nonlinear terms are given by the equations (27)–(29)

$$F_{\text{spring}} = -\left(2K\bar{\kappa}\frac{x_{01}^2}{L^2}\right)x + \left(\frac{2K\bar{\kappa}}{L^2}\right)x^3 \tag{27}$$

$$I_M = \frac{2\alpha\bar{\kappa}}{L}x\dot{x} \tag{28}$$

$$F_{\text{APA}} = \frac{2\alpha\bar{\kappa}}{L}xv. \tag{29}$$

The first nonlinear term represents the nonlinear mechanical spring force F_{spring}. This nonlinear restoring force is typical of duffing-type oscillators. In this particular case, the term proportional to x is negative and the term proportional to x^3 is positive, which corresponds to the existence of two stable equilibrium positions ($x_{\text{stable}} = \pm x_{01}$) and one unstable equilibrium position ($x_{\text{unstable}} = 0$) of the inertial mass.

Bistable oscillators can exhibit two different dynamic responses; one is the oscillation of the mass around one of the two stable equilibrium positions of the harvester ($\pm x_{01}$) without crossing the unstable position. This behavior is called intra-well motion [35]. The back and forth oscillation of the mass from one stable equilibrium position to another, by crossing the unstable position, is the second possible dynamic

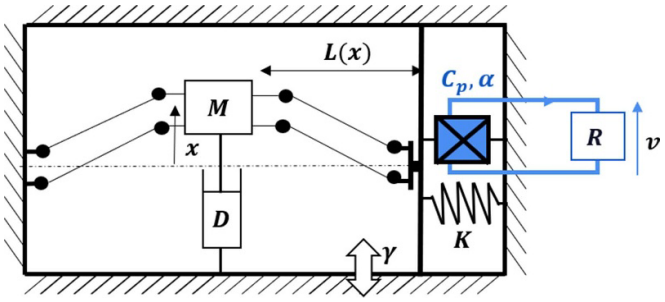

Figure 4. Schematic representation of the PRJ (Perfect Revolute Joint) lumped model used to describe the studied BPEH architecture by Huguet *et al* [37].

response. This type of response is called inter-well motion [35]. The latter is the oscillation that provides the high energy broadband response sought for this type of nonlinearity.

The second nonlinear term is the term representing the nonlinear electromechanical coupling (the piezoelectric direct effect where I_M is the current generated when the APA is deformed, and the piezoelectric inverse effect where F_{APA} is the force generated by the APA due to the voltage in its electrodes).

The nonlinearity in the electromechanical coupling corresponds to the fact that the piezoelectric element is compressed twice per period during the displacement of the dynamic mass in the case of inter-well motion. This frequency doubling phenomenon illustrates the nonlinear nature of the coupling, which is expressed by the products $x\dot{x}$ and xv in equation (26).

The advantage of the proposed lumped model described in (26) for this specific BPEH architecture is that it accounts for the effect of the tuning APA and the post-buckled beams' main strain contributions.

As previously mentioned, the difference with Huguet *et al*'s modelling approach [37] is the consideration of the tuning APA and the post-buckled beams' bending and axial compression stiffnesses. When the energy harvesting APA's stiffness is assumed to be small in regards to the tuning APA's stiffness ($K_2 \gg K$), and when the post-buckled beams' elasticity is not considered, the equations describing the dynamic behavior of the BPEH demonstrated by Huguet *et al* in [37] are obtained. Such a model amounts to consider the energy harvesting APA connected to the proof mass by Perfect Revolute Joints (PRJs) with infinitely rigid bars ($K_b = 0$, $K_a \to +\infty$, $\overline{\kappa} = 1$) instead of real beams characterized by the axial and flexural elasticities

$$\begin{cases} M\gamma = M\ddot{x} - 2K\frac{x_0^2}{L^2}x + \frac{2K}{L^2}x^3 + D\dot{x} + \frac{2\alpha}{L}xv \\ I = \frac{2\alpha}{L}x\dot{x} - C_p\dot{v} \end{cases}. \tag{30}$$

A schematic of the modelling approach proposed by Huguet *et al* [37] is illustrated in figure 4.

In this study, we propose an extension of Huguet *et al*'s [37] method for $\bar{\kappa} \leqslant 1$. The Huguet *et al*'s method will be referred to as the ideal PRJ model. One important conclusion stems from observing the difference between the ideal PRJ model and the model investigated in this paper: the tuning APA and post-buckled beams affect the dynamic behavior of the BPEH when $\bar{\kappa}$ is inferior to one.

2.3. Initial considerations/lumped model normalization

In order to determine the effect of the tuning APA and post-buckled beams' effect on performance, the influence of $\bar{\kappa}$ on key normalized parameters of the BPEH must be observed. The normalization of the equations is performed to obtain expressions of these key normalized parameters as a function of $\bar{\kappa}$, x_{01} and the rest of the structural parameters present in the equation system (26)

$$\begin{cases} \bar{\gamma} = \ddot{\bar{x}} + \frac{\omega_0^2}{\varepsilon^2}\frac{\bar{x}^3}{2} - \frac{\omega_0^2\bar{x}}{2} + \frac{\omega_0}{Q_m}\dot{\bar{x}} + k_m^2\frac{\omega_0^2}{\varepsilon^2}\bar{v}\bar{x} \\ \omega_r\bar{v} = \frac{\dot{\bar{x}}\bar{x}}{\varepsilon} - \dot{\bar{v}} \end{cases} \tag{31}$$

The normalized form of the equations describing the BPEH's response is given by (31) and the expressions of the normalized structural parameters of the BPEH that stem from it are expressed in (32)

$$\begin{cases} \bar{x} = \frac{x}{L} \\ \bar{v} = \frac{C_P v}{2\alpha\bar{\kappa}x_{0_1}} \\ \varepsilon = \frac{x_{01}}{L} \\ \omega_0 = \varepsilon\sqrt{\frac{4K\bar{\kappa}}{M}} \\ Q_m = \frac{\varepsilon\sqrt{4K\bar{\kappa}M}}{D} \\ k_m^2 = k_{m_{\text{APA}}}^2\bar{\kappa}^2 \\ \omega_r = \frac{1}{RC_p} \end{cases}. \tag{32}$$

The variable $k_{m\text{APA}}^2$ refers to the modified electromechanical coupling coefficient of the APA in a free–free configuration. The latter's expression is given by (33)

$$k_{m_{\text{APA}}}^2 = \frac{\alpha^2}{KC_p}. \tag{33}$$

This normalization allows the model to highlight parameters relevant to study VEHs' behaviors. Three parameters that are common to both linear and non-linear VEH are the characteristic pulsation ω_0, the quality factor Q_m and the electromechanical coupling coefficient k_m^2. An additional parameter ε that accounts for the buckling level is added for BPEHs.

It is worth noting that since the quality factor is a measure related to the system's damping, a variable that is challenging to forecast, its value will be considered fixed for the entire study.

Consequently, the normalization allows us to conclude that the elasticity factor $\bar{\kappa}$ given by (20) impacts the value of the characteristic pulsation ω_0 and the electromechanical coupling coefficient k_m^2.

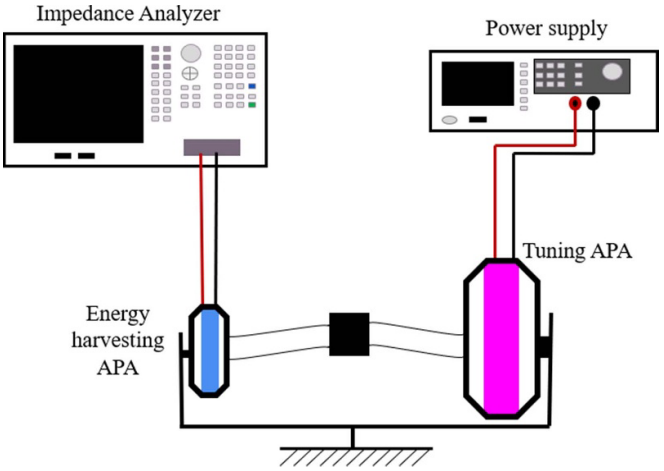

Figure 5. Experimental setup used for the impedance analysis tests carried out for the BPEH prototype.

3. Experimental validation

3.1. Prototype and test presentation

Figure 2 shows a prototype of the BPEH architecture studied.

The prototype incudes an APX4 steel block that was manufactured by the spark erosion process and that includes the beams, the inertial mass, as well as the spaces assigned for the APAs.

The APAs used for energy harvesting and tuning the buckling level are respectively the APA120S and the APA100M from Cedrat technologies.

Two types of experimental tests were carried out to explore the predictive capacity of the lumped model proposed.

The first type of tests are characterization tests that aim to compare the estimated key normalized parameters of the structure, based on the APAs' identified characteristics and beam geometry, to the ones obtained by impedance analysis. Following these tests, the structural parameters of the BPEH prototype are determined, and listed in table 3.

The second type of experimental tests consist of observing the displacement, power and phase responses of the BPEH prototype for a given sinusoidal ascending frequency sweep with a fixed acceleration amplitude. The results are then compared to the numerical estimations based on the lumped model.

3.2. BPEH impedance analysis tests

3.2.1. Experimental setup. The experimental setup for the impedance analysis tests is represented in figure 5.

A Keysight E4990A impedance analyzer is connected to the energy harvesting APA. The tests consist of varying the buckling level of the BPEH by imposing a constant voltage to the tuning APA through a Rhode and Schwartz NGE100 power supply, and then subjecting the BPEH to an impedance analysis for a low voltage of 5 mV around each stable position of the inertial mass.

The low level of voltage implies that the BPEH is subjected to a small excitation. In that regard, the observed response corresponds to small displacements of the inertial mass around the BPEH's stable equilibrium points. In prior references, these oscillations are referred to as low orbits [37] or intra-well movements [35].

Consequently, the non-linear terms of the proposed lumped model described by (31) can be neglected, leading to a linearized version of the electromechanical equations. The linearized version of the normalized equations is given by (34), with $\bar{u} = \bar{x} - \varepsilon$ (see equation (32)) and considering low values of normalized displacement as described in equation (35)

$$\begin{cases} \bar{\gamma} = \ddot{\bar{u}} + \omega_0^2 \bar{u} + \frac{\omega_0 \dot{\bar{u}}}{Qm} + k_m^2 \omega_0^2 \bar{v} \\ \bar{I} = \dot{\bar{u}} - \dot{\bar{v}} \end{cases} \tag{34}$$

$$\bar{u} \ll \varepsilon. \tag{35}$$

The analytical resolution of this system gives way to an expression of the theoretical normalized admittance $\breve{Y} = \frac{I}{jC_p\omega}$, similar to the one proposed by Kim *et al* [38]. This expression of the theoretical normalized admittance $\breve{Y}$, given by (36), is fitted to the experimental response in order to deduce the values of $(k_m^2,\ Q_m,\ \omega_0)$

$$\breve{Y} = 1 + \frac{k_m^2}{1 - \frac{\omega^2}{\omega_0^2} + \frac{j\omega}{Q_m\omega_0}}. \tag{36}$$

3.2.2. The elasticity factor experimental validation. The following study focuses on the estimated and experimentally determined values of k_m^2 and the characteristic frequency f_0, linked to the value of the characteristic pulsation ω_0 as shown in (37)

$$f_0 = \frac{\omega_0}{2\pi}. \tag{37}$$

The theoretical value of k_m^2 is calculated using the expression given by (32).

In addition, the values of the length L, width l_z and thickness l_y of the rectangular straight section of the post-buckled beams are provided in table 1. These dimensions allow us to determine the bending and axial extension stiffnesses K_b and K_a of the beams, using the formulas given by (38) and mentioned in [36], with E_{APX4} the young modulus of the steel used to manufacture the beams

$$(K_b, K_a) = \left(\frac{8E_{\mathrm{APX4}} l_z {l_y}^3}{(2L)^3}, \frac{E_{\mathrm{APX4}} l_z l_y}{L} \right). \tag{38}$$

Moreover, the electromechanical coupling coefficient $k^2_{m_{\mathrm{PRJ}}}$ of the APA120S used for energy harvesting was measured using the impedance analyzer on the energy harvesting APA in a free–free configuration, before installing it on the BPEH. This value is listed in table 1 as well.

Table 1. The measured values of the APAs and dimensions of the beams used in the BPEH prototype.

BPEH parameter	Symbol (unit if applicable)	Value
Length of the beams	$L\,(\mathrm{mm})$	35
Width of the beams	$l_z\,(\mathrm{mm})$	5
Thickness of the beams	$l_y\,(\mathrm{mm})$	0.2
APA120S coupling coefficient	$k^2_{m_{\mathrm{APA}}}$	0.11

Table 2. The theoretical values of the stiffnesses.

Theoretical parameter	Symbol (unit if applicable)	Value
APA120S stiffness	$K\left(\mathrm{N}\,\mu\mathrm{m}^{-1}\right)$	0.342
APA100M stiffness	$K_2\left(\mathrm{N}\,\mu\mathrm{m}^{-1}\right)$	1.8
Beam axial extension stiffness	$K_a\left(\mathrm{N}\,\mu\mathrm{m}^{-1}\right)$	6
Beam bending stiffness	$K_b\left(\mathrm{N\,m}^{-1}\right)$	196.87

Additionally, the nominal values of the energy harvesting APA's stiffness K and tuning APA's stiffness K_2 are listed in table 2.

The values of k^2_m and f_0 are measured for different values of the voltage imposed on the tuning APA, and thus, for different values of the buckling level x_{01}, computed based on the expression, given by (32), of x_{01} as a function of the resonant pulsation ω_0. The values of x_{01} are calculated using the theoretical value of the elasticity factor $\bar{\kappa}$. The measured values of the electromechanical coupling coefficient k^2_m for different buckling levels x_{01}, and thus for different levels of the voltage of the tuning APA, are represented in figure 6. Theory predicts a fixed value of the electromechanical coupling coefficient (see equation (32)), which is plotted in figure 6 as well. In addition, the electromechanical coupling coefficient computed from the PRJ model (figure 4), noted $k^2_{m_{\mathrm{PRJ}}}$, is plotted. The latter is equal to the electromechanical coupling coefficient of the APA120S in a free–free configuration $k^2_{m_{\mathrm{APA}}}$ as an elasticity factor $\bar{\kappa}$ equal to 1 is considered for the PRJ model.

According to the experimental results represented in figure 6, the measured values of the coupling coefficient k^2_m are far from the value $k^2_{m_{\mathrm{PRJ}}}$, which is the value attained when the elasticity factor $\bar{\kappa}$ is equal to one. Moreover, these values do not deviate from the theoretical value by more than 10% over the investigated range of buckling levels. Thus, the effect of the beams and tuning APA must be considered to have an accurate estimation of the electromechanical coupling coefficient of the BPEH k^2_m.

The relative error between the proposed model and experimental measurements may be due to measurement and manufacturing inaccuracies. It is observed that for high values of the voltage of the tuning APA, and thus low values of the apparent buckling level, the error reaches the uncertainty envelope's limit. This makes sense because for low resonance frequencies, the measured admittance is lower. Therefore, the current measured by the impedance analyzer reaches lower values that come close to the accuracy limit of the device, which justifies greater dispersion at low buckling levels.

Because the relative error between theory and experience is still less than 10%, the theoretical value of the elasticity factor is considered valid for the rest of the study.

3.2.3. The actual buckling level experimental validation.

Figure 7 represents the evolution of the actual buckling level x_{01} as a function of the voltage imposed on the tuning APA. A theoretical curve is plotted as well, using the theoretical buckling level x_{01} expression given by (19). An additional theoretical curve based on the formula provided by (19) for a null value of the bending stiffness K_b and an elasticity factor $\overline{\kappa}$ equal to 1 is presented, similar to the prior experimental validation. The latter will be referred to as the PRJ buckling level.

According to the experimental findings displayed in figure 7, the measured values of the apparent buckling level x_{01} differ from the PRJ apparent buckling level values by at least 0.4 mm. This underlines once more the importance of accounting for the impact of the tuning APA and the beams when making estimations.

The average relative error between the theoretical and the experimental results is equal to 12% for a tuning voltage lower than 70 V. For a tuning voltage V_2 higher than 70 V, the buckling level is too low and the assumption that the displacement of the inertial mass is very small with respect to the buckling level ($\bar{u} \ll \varepsilon$) is no longer valid, which explains why the experimental results differ from the model. In addition, at these low buckling levels, errors due to manufacturing defects, misalignments or asymmetries take on a greater relative importance. For a tuning voltage lower than 70 V, the average relative error is low enough to draw the conclusion that the lumped model's presumptions are reliable and enable accurate prediction of some BPEH properties before testing.

For a thorough validation of the proposed lumped model, oscillations from one stable position to another, referred to as high orbits [37] or inter-well motions [35] are studied in the next subsection. This type of response is relevant, as previously suggested, for energy harvesting applications.

3.3. BPEH response to an ascending sinusoidal frequency sweep

3.3.1. Experimental setup.

The experimental setup for the high orbit tests is represented in figure 8.

The BPEH prototype is fixed on an electromagnetic shaker driven by a power amplifier. The shaker's acceleration is monitored by an accelerometer fixed on the shaker and connected to a dSpace controlling board, which drives the power amplifier in a closed loop to control the acceleration amplitude with a PI controller.

The displacement, velocity and acceleration of the inertial mass are monitored with a differential laser vibrometer also connected to the dSpace controlling board. The tuning APA is driven by a power supply that imposes a constant voltage; the buckling level of the beams is thus fixed for the duration

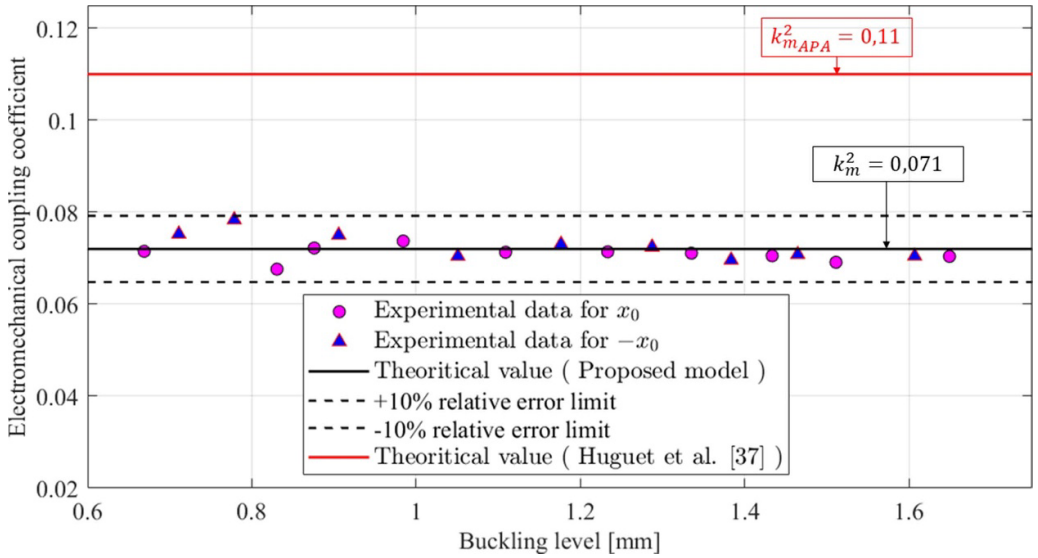

Figure 6. The evolution of the measured electromechanical coupling coefficient for different buckling levels (magenta circles and blue triangles) and the theoretical (black solid line) and PRJ [37] model (red solid line) values of the electromechanical coupling coefficient: $k^2_m = \bar{\kappa}^2 k^2_{m_{\text{APA}}}$ and $k^2_{m_{\text{PRJ}}} = k^2_{m_{\text{APA}}}$.

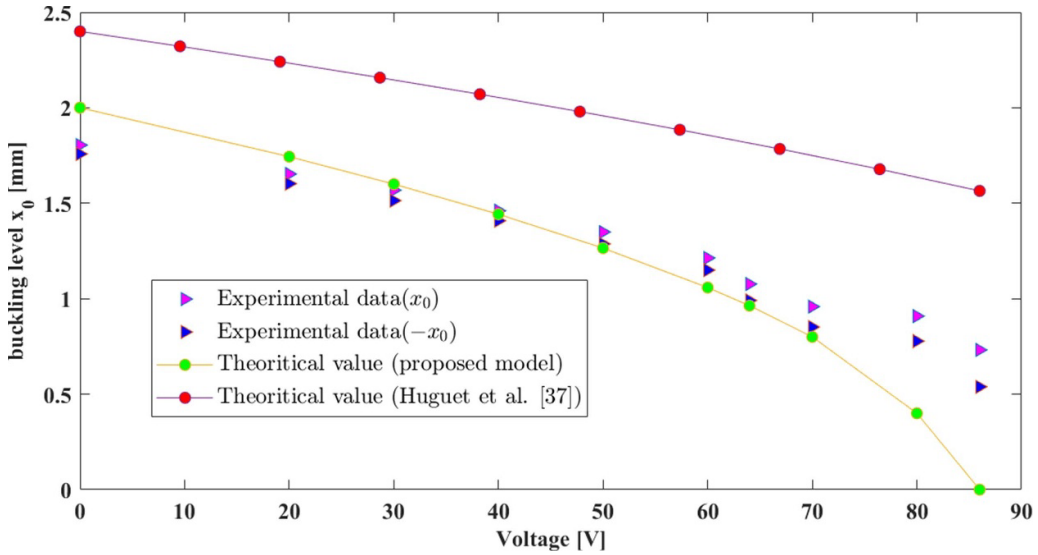

Figure 7. The evolution of the measured, theoretical and PRJ [37] actual buckling level for different values of the voltage V_2 applied through the tuning APA.

of the experiments. The energy harvesting APA is connected to a programmable resistance load, linked to the dSpace controlling board that can adjust its value. The voltage across the energy harvesting APA is also monitored with a voltage follower connected to the dSpace board.

3.3.2. Experimental validation results. This experiment consists of observing the displacement amplitude, the harvested power and the phase lag between the displacement and input acceleration of the harvester for the BPEH prototype represented in figure 2, when the latter is in high orbit, for different values of the buckling level. The numerical responses obtained by using the lumped model proposed and a numerical differential equation solver on MATLAB are then compared to the experimental test response, for the fixed initial conditions expressed in (39)

$$\begin{pmatrix} \bar{x}(t=0) \\ \dot{\bar{x}}(t=0) \\ \bar{v}(t=0) \end{pmatrix} = \begin{pmatrix} \varepsilon \\ 0 \\ 0 \end{pmatrix}. \tag{39}$$

The acceleration imposed is an ascending frequency sweep with an acceleration amplitude γ that ranges from 30 Hz to 90 Hz. The sweep rate chosen is of 0.1 Hz per second, which ensures a quasi-static evolution of the acceleration frequency.

The identified parameters of the BPEH prototype represented in figure 2 are listed in table 3. The tested buckling level

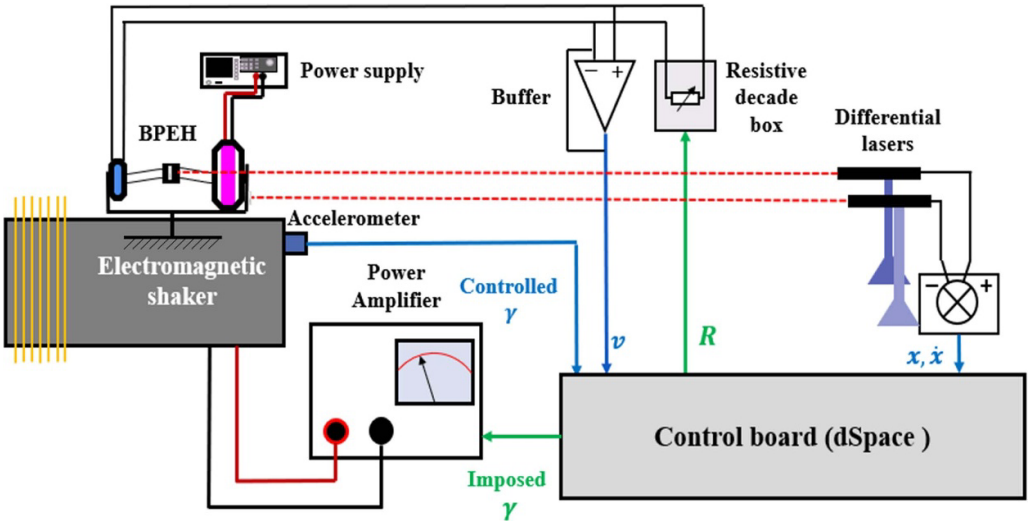

Figure 8. Schematic representation of the experimental setup used to observe the response of the BPEH prototype to an ascending sinusoidal frequency sweep.

Table 3. The identified structural parameters of the BPEH prototype used for the experimental validation.

Parameter	Symbol (unit if applicable)	Value
Mass frame distance	$L\,(\mathrm{mm})$	35
Inertial mass	$M\,(\mathrm{g})$	6
Buckling level	$x_0\,(\mathrm{mm})$	{0.7, 0.85, 0.975, 1.05, 1.75}
Electromechanical coupling coefficient	k_m^2	0.071
Quality factor	Q_m	160
Characteristic frequency	$f_0\,(\mathrm{Hz})$	{47,57,65,70,78}
Resistance load	$R\,(\Omega)$	1000
Acceleration amplitude	$\gamma_M\ \left(\mathrm{m}\cdot\mathrm{s}^{-2}\right)$	5
Acceleration frequency range	$f\ (\mathrm{Hz})$	[30,90]

values, chosen resistance load as well as the acceleration amplitude and frequency range can be found in table 3 as well.

The experimental and numerical inter-well responses of the BPEH prototype for different buckling level values are shown in figure 9.

The calculated relative error between theoretical model and experiment is computed using the next equation where $n_{x_{01}}$ and n_{f} are the number of buckling levels and frequencies tested. P_{th} and P_{exp} are theoretical mean power and experimental mean power respectively. D_{th} represents the theoretical displacement amplitude and D_{exp} the experimental displacement amplitude. The average relative error is equal to 5.86% for the model presented in this article. For the ideal PRJ model, this relative error is equal to 14.18%

$$\text{Relative error} = \frac{1}{2n_{x_{01}}n_{\mathrm{f}}}\sum_{n_{x_{01}}}\sum_{n_{\mathrm{f}}}\left(\frac{|P_{\mathrm{th}}-P_{\mathrm{exp}}|}{P_{\mathrm{exp}}}+\frac{|D_{\mathrm{th}}-D_{\mathrm{exp}}|}{D_{\mathrm{exp}}}\right). \quad (40)$$

Consequently, the model assumptions can be considered more predictive than the ones proposed by Huguet *et al* in [37] or what is referred to as the ideal PRJ model represented in figure 4. Furthermore, The response of the harvester for different buckling levels is coherent with what was predicted theoretically by Morel *et al* [39]; for a specific driving frequency f, the output power and displacement are higher for higher buckling levels. However, the maximum power output attained at the critical frequency is lower for higher buckling levels.

This leads to a very relevant conclusion regarding this type of BPEH architecture; varying the buckling level can allow a tuning of the BPEH's performance as it acts on the power harvested and on the bandwidth of its high orbit response. This tunability can also be exploited for orbit jump strategies, as suggested by Saint-Martin *et al* [40] for the prototype presented in this paper.

4. The effect of the elasticity factor $\bar{\kappa}$ on a BPEH's dynamic performance

4.1. Numerical simulation presentation

In this section, we investigate the effect of the elasticity factor $\bar{\kappa}$ on the inter-well response [35] or high orbit response [39] of a given BPEH. The dynamic response of the BPEH to a sinusoidal ascending frequency sweep with a high enough

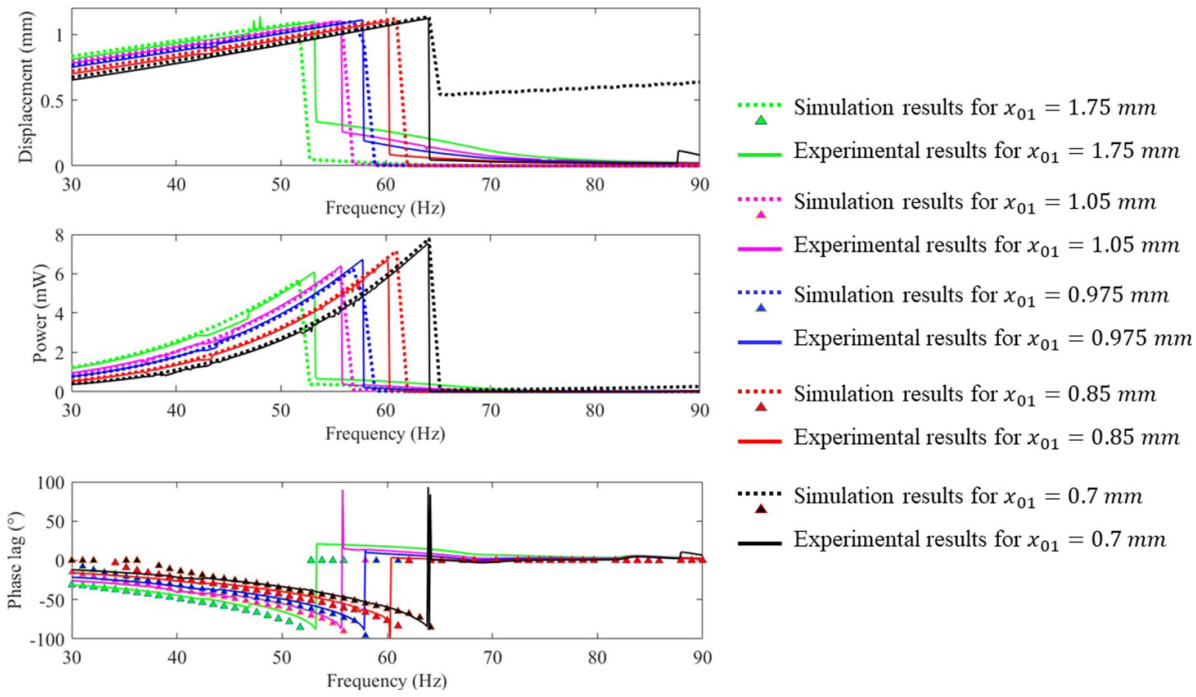

Figure 9. Displacement, power and phase lag responses of the BPEH prototype tested for an ascending frequency sweep with a fixed acceleration $\gamma = 5\ \mathrm{m \cdot s^{-2}}$ and a fixed resistance load $R = 1\ \mathrm{k\Omega}$.

acceleration amplitude γ to cause this high orbit is investigated using numerical simulations.

The numerical simulations are run using the lumped model for different values of the elasticity factor $\bar{\kappa}$, in the case of a BPEH prototype with similar features as the one used for the experimental validation presented in the previous section. These simulations are carried out for an ascending frequency sweep with a fixed acceleration $\gamma = 20\ \mathrm{m\,s^{-2}}$.

The resistance load R is fixed in regards to the value of the damping ratio β, described in [39], which represents the ratio between the electric and mechanical damping of the BPEH.

The value of the resistance load R is chosen so as to have the damping ratio β set to the closest value to 1 when the driving frequency is equal to the cut-off frequency f_c of the high orbit response for the set acceleration amplitude. The cut-off frequency f_c, as described in [39], is the frequency at which the high orbit ceases to exist. When the electric damping ratio β is set to 1, the electric damping and mechanical damping of the BPEH are equal. Consequently, the maximum power of the BPEH is reached and is equal to P_{lim} which is given by (41)

$$P_{\mathrm{lim}} = \frac{M\gamma^2 Q_m}{8\omega_0}\ . \tag{41}$$

The numerical results presented are obtained using a numerical differential equation solver on MATLAB for the fixed initial conditions expressed in (39).

The parameters set for the numerical simulations are given by table 4.

Table 4. The *BPEH structural parameters set for the numerical simulation.*

Variable	Quantity (unit if applicable)	Value
M	Inertial mass (g)	5
x_{01}	Actual buckling level (mm)	0.7
Q_m	Mechanical quality factor	100
L	Mass-frame distance (mm)	35
K	Energy harvesting APA stiffness (N μm^{-1})	0.342
$k^2_{m_{\mathrm{APA}}}$	APA120S coupling coefficient	0.11
γ_M	Driving acceleration amplitude (g)	2
f	Driving frequencies tested (Hz)	[40, 300]
$\bar{\kappa}$	Elasticity factors tested (-)	{0.1,0.3,0.5,0.7,0.9,1}

It is worth noting that the actual buckling level x_{01} is kept at a constant value in these simulations. This can be achieved by modifying the voltage that goes through the tuning APA for each value of the elasticity factor $\bar{\kappa}$. For simplicity's sake, the quality factor's value is considered to be constant regardless of the beam geometry or the tuning APA used.

Consequently, the elasticity factor variation only affects the electromechanical coupling level and resonant frequency of the harvester studied, as described by the equation system (32).

4.2. Numerical simulation results and physical interpretations

The simulation results are the displacement amplitude, the harvested power and the phase lag between the displacement and

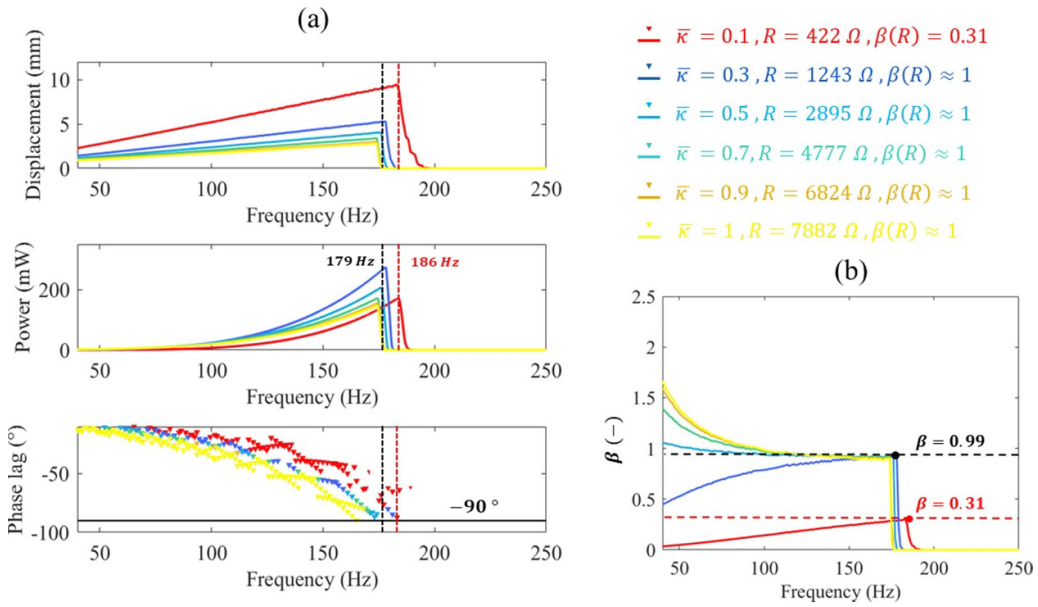

Figure 10. (a) Displacement, power and phase lag responses of the BPEH to an ascending frequency sweep with a fixed acceleration $\gamma = 20\ \mathrm{m \cdot s^{-2}}$ for different elasticity factor values $\overline{\kappa} \in [0.1, 1]$ (b) Damping ratio β as a function of the driving frequency f for different values of the elasticity factor $\overline{\kappa} \in [0.1, 1]$.

input displacement of the harvester, for different values of the elasticity factor $\bar{\kappa}$. These results are shown in figure 10(a). In addition, the evolution of the damping ratio β, expressed in (42) was plotted as a function of the elasticity factor and driving frequency. This result is shown in figure 10(b)

$$\beta = \frac{k_m^2 Q_m x^2 (RC_0\omega_0)^2}{4x_0^2\left(1 + 4(RC_0\omega_0)^2\left(\frac{2\pi f}{\omega_0}\right)^2\right)} \tag{42}$$

β equal to 1 is obtained at the cut-off frequency f_c with a resistive load provided the value of $k_m^2 Q_m$ surpasses a threshold determined by the generator's geometric parameters and the level of acceleration. This threshold can be determined using the simple model proposed by Morel *et al* [39], which gives way to the condition described (43)

$$k_m^2 Q_m \geqslant \frac{12\left(\frac{2\pi f_c}{\omega_0}\right)}{1 + 2\left(\frac{2\pi f_c}{\omega_0}\right)^2}\ . \tag{43}$$

If the value of $k_m^2 Q_m$ is high enough in regards to the previously described condition, the electric damping ratio β reaches 1 when the phase between the displacement and the acceleration is equal to $-90°$, and thus, when the driving frequency is equal to the cut-off frequency. In this case, the first takeaway is that the cut-off driving frequency f_c remains the same when varying the elasticity factor, despite it having an effect on the electromechanical coupling k_m^2 and the resonant frequency of the BPEH. The elasticity factor variation does, however, have an effect on the harvested power and displacement amplitudes. When the elasticity factor is smaller, these amplitudes rise, implying that more power is harvested since the amplitude of the inertial mass's displacement is larger. This is because lower elasticity factor values imply more flexible structure when compared to the stiffness of the energy harvesting APA. Moreover, we notice in figure 10(a) that the harvested power at the cut-off frequency increases as $\bar{\kappa}$ decreases provided $k_m^2 Q_m$ is high enough and β equal to 1 is reached. This is because P_{lim} is inversely proportional to ω_0 (see equation (41)) and ω_0 is proportional to the square root of $\bar{\kappa}$ (see equation (32)).

If $k_m^2 Q_m$ is too low, which is the case for $\bar{\kappa} = 0.1$, a value of electric damping ratio β of 1 cannot be reached at the cut-off frequency with a resistive load. In this case, the maximum harvested power does not reach P_{lim} and the harvested power at the cut-off frequency decreases when $\bar{\kappa}$ increases. At a certain point, the degradation caused by lowering the elasticity factor is therefore not beneficial. Additionally, a change in the cut-off frequency due to the difference in damping ratios is noticed.

These simulation results can be further explained theoretically. The value of P_{lim} is higher when the value of the elasticity factor $\bar{\kappa}$ is lower. This can be concluded by observing the formula given by (41) since the value of the resonant pulsation ω_0 is lower when the elasticity factor $\bar{\kappa}$ decreases, as shown by equation (32). The expression given by (41) can therefore be rewritten as a function of the elasticity factor $\bar{\kappa}$ to highlight this further, by considering the variable $\omega_{0_{\mathrm{PRJ}}}$ which is equal to $\varepsilon\sqrt{\frac{4K}{M}}$ and corresponds to the resonant pulsation of the BPEH when the perfect revolute joint model is considered. This expression is given by (44)

$$P_{\mathrm{lim}} = \frac{M\gamma^2 Q_m}{8\omega_{0_{\mathrm{PRJ}}}\sqrt{\bar{\kappa}}}\ . \tag{44}$$

However, the harvested power can only reach P_{lim} if the condition described by (43) is satisfied. Satisfying this

condition implies that the damping ratio can reach 1 when the driving frequency is equal to the cut-off frequency. For the condition described by (43) to be satisfied, the coupling coefficient k_m^2 must be high enough, since the quality factor Q_m is assumed to be independent of $\bar{\kappa}$. A decrease in the value of the elasticity factor $\bar{\kappa}$ implies a decrease in the value of the coupling coefficient k_m^2, as shown by the expressions given by (32).

Consequently, in order for the harvested power to reach P_{lim} at the cut-off frequency the elasticity factor $\bar{\kappa}$ must be equal to the lowest value that guarantees that the criterion given by (43) is satisfied. This optimal value ensures that the damping ratio β can reach 1 at the cut-off frequency f_c and that the harvested power reaches P_{lim} at this particular frequency.

The optimal value of $\bar{\kappa}$ can be determined thanks to the next equation that expresses the threshold value of (45) as a function of $\bar{\kappa}$ using the equation (32)

$$\bar{\kappa}^2 k_{m_{\text{APA}}}^2 Q_m = \frac{12\sqrt{\bar{\kappa}}\left(\frac{2\pi f_c}{\omega_{0_{\text{PRJ}}}}\right)}{\bar{\kappa}+2\left(\frac{2\pi f_c}{\omega_{0_{\text{PRJ}}}}\right)^2}. \tag{45}$$

Since f_c is constant when $\beta = 1$ is reached for a given quality factor Q_m and acceleration level γ, the equation can be solved with respect to $\bar{\kappa}$ for our architecture. Considering $Q_m = 160$ and $\gamma = 20\,\text{m}\,\text{s}^{-2}$, which imply a cut-off frequency of 179 Hz for our configuration, we find an optimal value of $\bar{\kappa}$ equal to 0.21 by solving the equation with $\omega_{0_{PRJ}} = 332.19\,\text{rad}\cdot\text{s}^{-1}$. Moreover, the optimal value of $\bar{\kappa}$ can be found through numerical simulations by varying $\bar{\kappa}$ and observing the threshold where $\beta = 1$ is reached. The optimal value is also found to be equal to 0.21 for the BPEH studied at $\gamma = 20\,\text{m}\,\text{s}^{-2}$. The value of the threshold $k_m^2 Q_m$ is equal to 0.5 in our case.

Considering the value of the elasticity factor when designing the BPEH is thus necessary. The optimal value of the elasticity factor is the minimum value of $\bar{\kappa}$ for which $k_m^2 Q_m$ is high enough to reach $\beta = 1$. The geometry of the beams and tuning APA must consequently be chosen in regards to the optimal value.

5. Conclusion

This paper presents a predictive lumped model suited for a type of BPEH architecture that uses post-buckled beams to create bistability, and APAs to harvest the vibration energy and, eventually, tune the BPEH's buckling level. This model accounts for the effect of the buckled beams' bending and axial extension stiffnesses, as well as the effect of the tuning APA. The lumped model proposed is established using Euler–Lagrange equations, and a system describing the mechanical and electrical response of the dynamic system's behavior are found. The theoretical results that stem from the lumped model proposed to show that, while the bending stiffness of the beams has no effect on the dynamic response, the axial extension stiffness and the tuning APA's stiffness impact the latter and can be taken into account using an elasticity factor.

Experimental tests were carried out using a BPEH prototype with the studied architecture. These tests reveal that the numerical and theoretical results are in good agreement as they show an average error below 6%. Furthermore, a numerical study is made to investigate the effect of the elasticity factor on the high orbit response of the BPEH. The results of this study show that for a given BPEH, there's an optimal value of the elasticity factor that ensures a maximum power output while maintaining the operating frequency band.

By incorporating the elasticity factor, the suggested model improves the understanding of the effect of the post-buckled beams and tuning APA on the dynamic response of the BPEH. The suggested lumped model's predictive capability therefore simplifies the design of BPEHs for optimal dynamic performance. Finally, the inclusion of the tuning APA's effect in the lumped model facilitates the simulation of orbit jump scenarios, made to improve the BPEH's power response, using a rapid buckling level variation, such as the one described in Huguet *et al*'s [37] and Saint-Martin *et al*'s [40] contributions.

Data availability statement

The data cannot be made publicly available upon publication because they are not available in a format that is sufficiently accessible or reusable by other researchers. The data that support the findings of this study are available upon reasonable request from the authors.

Acknowledgments

This project has received funding from the European Union's Horizon 2020 research and innovation program under Grant Agreement No. 862289.

ORCID iDs

Aya Benhemou https://orcid.org/0009-0006-1842-7426
David Gibus https://orcid.org/0000-0001-7529-5868
Adrien Morel https://orcid.org/0000-0002-5603-4029
Quentin Demouron https://orcid.org/0009-0009-7686-8379
Camille Saint-Martin https://orcid.org/0000-0002-5719-4411
Ludovic Charleux https://orcid.org/0000-0003-3533-2438
Adrien Badel https://orcid.org/0000-0001-7295-5381

References

[1] Rashid B and Rehmani M H 2016 Applications of wireless sensor networks for urban areas: a survey *J. Netw. Comput. Appl.* **60** 192–219
[2] Kandris D, Nakas C, Vomvas D and Koulouras G 2020 Applications of wireless sensor networks: an up-to-date survey *Appl. Syst. Innov.* **3** 14
[3] Teresa Penella M, Albesa J and Gasulla M 2009 Powering wireless sensor nodes: primary batteries versus energy harvesting *2009 IEEE Intrumentation and Measurement Technology Conf.* (IEEE) pp 1625–30
[4] Singh J, Kaur R and Singh D 2021 Energy harvesting in wireless sensor networks: a taxonomic survey *Int. J. Energy Res.* **45** 118–40

[5] Mohanty A, Parida S, Behera R K and Roy T 2019 Vibration energy harvesting: a review *J. Adv. Dielectr.* **9** 1930001

[6] Zhang Y, Luo A, Wang Y, Dai X, Lu Y and Wang F 2020 Rotational electromagnetic energy harvester for human motion application at low frequency *Appl. Phys. Lett.* **116** 053902

[7] Le C P and Halvorsen E 2012 MEMS electrostatic energy harvesters with end-stop effects *J. Micromech. Microeng.* **22** 074013

[8] Li M, Luo A, Luo W and Wang F 2022 Recent progress on mechanical optimization of MEMS electret-based electrostatic vibration energy harvesters *J. Microelectromech. Syst.* **31** 726–40

[9] Nechibvute A, Chawanda A and Luhanga P 2012 Piezoelectric energy harvesting devices: an alternative energy source for wireless sensors *Smart Mater. Res.* **2012** 1–13

[10] Roundy S and Wright P K 2004 A piezoelectric vibration based generator for wireless electronics *Smart Mater. Struct.* **13** 1131–42

[11] Roundy S, Wright P K and Rabaey J 2003 A study of low level vibrations as a power source for wireless sensor nodes *Comput. Commun.* **26** 1131–44

[12] Tang L, Yang Y and Soh C K 2010 Toward broadband vibration-based energy harvesting *J. Intell. Mater. Syst. Struct.* **21** 1867–97

[13] Daqaq M F, Masana R, Erturk A and Dane Quinn D 2014 On the role of nonlinearities in vibratory energy harvesting: a critical review and discussion *Appl. Mech. Rev.* **66** 040801

[14] Shim H-K *et al* 2022 On a non-linear broadband piezoelectric energy harvester with a coupled beam array *Appl. Energy* **328** 120129

[15] Zou D, Liu G, Rao Z, Zi Y and Liao W-H 2021 Design of a broadband piezoelectric energy harvester with piecewise non-linearity *Smart Mater. Struct.* **30** 085040

[16] Harne R L and Wang K W 2013 A review of the recent research on vibration energy harvesting via bistable systems *Smart Mater. Struct.* **22** 023001

[17] Jiang J, Liu S, Feng L and Zhao D 2021 A review of piezoelectric vibration energy harvesting with magnetic coupling based on different structural characteristics *Micromachines* **12** 436

[18] Lu Q, Scarpa F, Liu L, Leng J and Liu Y 2018 An E-shape broadband piezoelectric energy harvester induced by magnets *J. Intell. Mater. Syst. Struct.* **29** 2477–91

[19] Yang W and Towfighian S 2017 A hybrid non-linear vibration energy harvester *Mech. Syst. Signal Process.* **90** 317–33

[20] Pan J, Qin W and Deng W 2019 Promote efficiency of harvesting vibration energy by tailoring potential energy with addition of magnets *AIP Adv.* **9** 075323

[21] Zhang X, Yang W, Zuo M, Tan H, Fan H, Mao Q and Wan X 2018 An arc-shaped piezoelectric bistable vibration energy harvester: modeling and experiments *Sensors* **18** 4472

[22] Arrieta A F, Hagedorn P, Erturk A and Inman D J 2010 A piezoelectric bistable plate for non-linear broadband energy harvesting *Appl. Phys. Lett.* **97** 104102

[23] Masana R and Daqaq M F 2012 Energy harvesting in the super-harmonic frequency region of a twin-well oscillator *J. Appl. Phys.* **111** 044501

[24] Chen K, Ding X, Tian L, Shen H, Song R, Bian Y and Yang Q 2023 An M− shaped buckled beam for enhancing non-linear energy harvesting *Mech. Syst. Signal Process.* **188** 110066

[25] Qian F, Hajj M R and Zuo L 2020 Bio-inspired bi-stable piezoelectric harvester for broadband vibration energy harvesting *Energy Convers. Manage.* **222** 113174

[26] Vangbo M 1998 An analytical analysis of a compressed bistable buckled beam *Sens. Actuators* **69** 212–6

[27] Camescasse B, Fernandes A and Pouget J 2013 Bistable buckled beam: elastica modeling and analysis of static actuation *Int. J. Solids Struct.* **50** 2881–93

[28] Yan W, Yu Y and Mehta A 2019 Analytical modeling for rapid design of bistable buckled beams *Theor. Appl. Mech. Lett.* **9** 264–72

[29] Saif M T A 2000 On a tunable bistable MEMS-theory and experiment *J. Microelectromech. Syst.* **9** 157–70

[30] Cottone F, Gammaitoni L, Vocca H, Ferrari M and Ferrari V 2012 Piezoelectric buckled beams for random vibration energy harvesting *Smart Mater. Struct.* **21** 035021

[31] Kim D, Hewa-Kasakarage N N and Hall N A 2014 A theoretical and experimental comparison of 3-3 and 3-1 mode piezoelectric microelectromechanical systems (MEMS) *Sens. Actuators* **219** 112–22

[32] Kardarakos G C, Chrysochoidis N A, Varelis D and Saravanos D A 2023 Numerical and experimental investigation of the energy harvesting performance of electromechanically coupled piezoelectric prestressed beams subjected to non-linear vibrations *Smart Mater. Struct.* **32** 035019

[33] Zou H-X, Zhang W-M, Wei K-X, Li W-B, Peng Z-K and Meng G 2016 A compressive-mode wideband vibration energy harvester using a combination of bistable and flextensional mechanisms *J. Appl. Mech.* **83** 121005

[34] Liu W, Formosa F, Badel A and Hu G 2017 A simplified lumped model for the optimization of post-buckled beam architecture wideband generator *J. Sound Vib.* **409** 165–79

[35] Liu W Q, Badel A, Formosa F, Wu Y P and Agbossou A 2013 Novel piezoelectric bistable oscillator architecture for wideband vibration energy harvesting *Smart Mater. Struct.* **22** 035013

[36] Benhemou A *et al* 2022 Design approach for post-buckled beams in bistable piezoelectric energy harvesters *2022 Wireless Power Week (WPW)* (IEEE) pp 136–40

[37] Huguet T, Lallart M and Badel A 2019 Orbit jump in bistable energy harvesters through buckling level modification *Mech. Syst. Signal Process.* **128** 202–15

[38] Kim M, Hoegen M, Dugundji J and Wardle B L 2010 Modeling and experimental verification of proof mass effects on vibration energy harvester performance *Smart Mater. Struct.* **19** 045023

[39] Morel A, Charleux L, Demouron Q, Benhemou A, Gibus D, Saint-Martin C, Carré A, Roux E, Huguet T and Badel A 2022 Simple analytical models and analysis of bistable vibration energy harvesters *Smart Mater. Struct.* **31** 105016

[40] Saint-Martin C *et al* 2023 Optimized and robust orbit jump for non-linear vibration energy harvesting *Nonlinear Dyn.* (https://doi.org/10.1007/s11071-023-09188-x)